Research
Deep Matter & Energy—Article

Carbonation of Chrysotile under Subduction Conditions

Mihye Kong [a], Yongjae Lee [a,b,*]

[a] Department of Earth System Sciences, Yonsei University, Seoul 03722, Korea
[b] Center for High Pressure Science and Technology Advanced Research (HPSTAR), Shanghai 201203, China

ABSTRACT

In order to understand the role of serpentine minerals in the global carbon cycle, high-pressure X-ray diffraction (XRD) experiments were performed on chrysotile ($Mg_3Si_2O_5(OH)_4$) using carbon dioxide (CO_2) as a pressure medium. Synchrotron XRD patterns revealed the formation of magnesite and high-pressure chrysotile after heating at 170 °C for 1 h at 2.5(1) GPa. The Rietveld refinement suggests that the unit cell composition of the original chrysotile changes to $Mg_{2.4(1)}Si_2O_5(OH)_{2.4(1)}$ upon the formation of magnesite, which appears to be driven by the dehydrogenation of the innermost hydroxyl group, OH3, and the rearrangement of magnesium (Mg) at the M1 site, leading to the formation of metastable monodehydroxylated chrysotile. Metastable chrysotile is observed up to 5.0(1) GPa and 500 °C, which corresponds to the slab Moho geotherms for the South Sumatra and Ryukyu subduction zone. After recovery to ambient conditions, the characteristic fibrous morphology of the original chrysotile was found to have changed to an earthy form. These results can help us to understand deep carbon cycling along the subduction zones, and may prompt the design of a novel method of asbestos detoxification using pressure and temperature.

© 2019 THE AUTHORS. Published by Elsevier LTD on behalf of Chinese Academy of Engineering and Higher Education Press Limited Company. This is an open access article under the CC BY-NC-ND license (http://creativecommons.org/licenses/by-nc-nd/4.0/).

1. Introduction

Understanding the carbon distribution in the Earth's interior is crucial in understanding the global carbon cycle, which includes carbon dioxide (CO_2) in the atmosphere and hydrosphere [1,2]. The parts of the global carbon cycle that involve the solid Earth include CO_2 degassing along mid-ocean ridges and arc-volcanism, and CO_2 storage in the oceanic crust and mantle via the hydrothermal alteration of basalts and the serpentinization of mantle peridotites [3,4]. While the former processes release volatile components into surface and subsurface reservoirs, the subduction of the oceanic lithosphere is a major inlet supplying volatiles to mantle reservoirs [5,6]. The global average CO_2 content in the oceanic sediment entering subduction zones is estimated to be about (3.01 ± 1.44) wt% [7]. It is estimated that fresh mid-ocean ridge basalt (MORB) contains about 0.15 wt% CO_2, but during alteration and seafloor weathering, the CO_2 content of the upper 600 m of the oceanic crust may increase to about 3 wt% and the average CO_2 gain of the entire crustal section is elevated to about 0.4 wt% [8].

The subducting lithosphere contains an average of about 2 wt% CO_2 in the uppermost volcanic section and 100–5000 ppm (1 ppm = 10^{-6}) CO_2 throughout the remaining approximately 7 km of crust [9]. During this process, metamorphic re-equilibration of slab carbon with oxidizing fluids released during serpentine dehydration under sub-arc conditions would facilitate carbonation reactions to convert most slab carbon to carbonate minerals [10]. Carbonate minerals can also form during hydrothermal carbonation and weathering of serpentinites [11]. Slab dehydration is known to occur between 40 and 200 km, which is related to the stability of various hydrous phases such as serpentine, chlorite, amphiboles, lawsonite, and mica [12–15].

A considerable quantity of carbon may survive beyond slab dehydration and be subducted into the deep mantle [6,16–18]. Earth's mantle is likely the largest carbon reservoir of the planet, and may surpass all other carbon reservoirs on the surface or in subsurface environments. Magnesite ($MgCO_3$) is considered to be one of the major candidates to host carbon in the Earth's mantle [19].

Serpentine minerals are major constituents of the hydrated upper mantle of oceanic plates and of the mantle wedge overlying subduction zones [20,21]. They are thus considered to play a major role in the cycling of water and volatile elements in the upper

* Corresponding author.
  E-mail address: yongjaelee@yonsei.ac.kr (Y. Lee).

mantle [20,22] and in tectonic and seismic processes [23–26]. Serpentine minerals are characterized by a 1:1 layer structure consisting of octahedral and tetrahedral sheets. Among the serpentine minerals, chrysotile ($Mg_3Si_2O_5(OH)_4$), also known as white asbestos, characteristically forms the cylindrical fiber crystals that give asbestos its characteristic properties (Fig. 1). The fibers are achiral, being rolled up around the *a*-axis (normal chrysotile) or, less commonly, around the *b*-axis (parachrysotile). This magnesium hydroxide silicate exhibits a scroll-like bilayer consisting of a tetrahedral $[SiO_4]^{4-}$ silicate sheet (*T*) spreading along the surface of mutual contact with a trioctahedral $[Mg_3O_2(OH)_4]^{2-}$ brucite-like sheet (*O*) (Fig. 1(a)). Chrysotile occurs in regions ranging from surficial or near-surficial environments to some depths when subducted [27]. The upper limit of the chrysotile stability field has been reported to be up to 600 °C and/or 100 km in depth along cold subduction zones [28].

To understand the interaction between CO_2 and subducting minerals, we performed high-pressure and high-temperature X-ray diffraction (XRD) experiments on chrysotile up to 5.0(1) GPa and 500 °C using CO_2 as the pressure-transmitting medium (PTM).

2. Materials and methods

High-pressure and high-temperature experiments on chrysotile (obtained from Quebec, Canada, NMMH 156082 from the Smithsonian Institution) were performed at beamline 10C at the Pohang Accelerator Laboratory (PAL), Korea, and at beamline 16BMD of the High-Pressure Collaborative Access Team (HPCAT) at the Advanced Photon Source (APS) at the Argonne National Laboratory, USA. At the 16BMD beamline, a monochromic X-ray beam with a wavelength of 0.4959(1) Å and a diameter of 90 μm was used, and a MAR345 detector was used to measure the XRD patterns at a sample-to-detector distance of about 299 mm in order to cover 2-theta up to about 30° with an exposure time of 300 s. At the PAL, a similar setup was employed using a monochromic X-ray beam with a wavelength of 0.6199(1) Å and a diameter of

200 μm. The position of the incident beam, sample-to-detector distance, and detector tilt were determined using a LaB_6 standard (SRM 660).

A modified Merrill–Bassett diamond anvil cell (DAC) was used for the high-pressure experiments, equipped with two type-I diamond anvils (culet diameter of 700 μm) and tungsten-carbide supports. A stainless-steel foil of 200 μm thickness was pre-indented to a thickness of about 130 μm, where a central hole was obtained by means of electro-spark erosion. The powdered sample of chrysotile was placed in the gasket hole together with some ruby chips for *in situ* pressure measurements. Ambient pressure data were collected first on the dry sample inside the DAC. Subsequently, solid CO_2 was loaded on the packed powder sample in the DAC under low temperature cooled with liquid nitrogen and sealed to the first pressure point. For *ex situ* heating, the DAC was placed in an oven for 1 h and then cooled to room temperature. For *in situ* heating, we used a cylinder-type DAC consisting of a ring-shaped ceramic heater. The thickness of the platinum wire was 0.3 mm, and a resistance of 0.6 Ω was used in order to employ the wire as a heating element.

The pressure of the sample in the DAC was measured by detecting the shift in the R1 emission line of the included ruby chips (precision: ±0.05 GPa) [29]. The sample was typically equilibrated for about 10 min in the DAC at each measured pressure. After each powder diffraction pattern was collected, the pressure was increased in increments of about 0.5 GPa.

Pressure-dependent changes in the unit cell lengths and volume were derived from a series of whole-profile fitting procedures using the high-pressure data and the general structure analysis system (GSAS) suite of programs [30,31]. The background was fitted with a Chebyshev polynomial with ≤ 20 coefficients, and the pseudo-Voigt profile function proposed by Thompson et al. [32] was used to model the observed Bragg peaks. The Rietveld refinement was then performed using data measured under ambient conditions after heating at 170 °C for 1 h at 2.5(1) GPa. The isotropic displacement factors of the structural models were refined by grouping the framework tetrahedral and octahedral atoms and
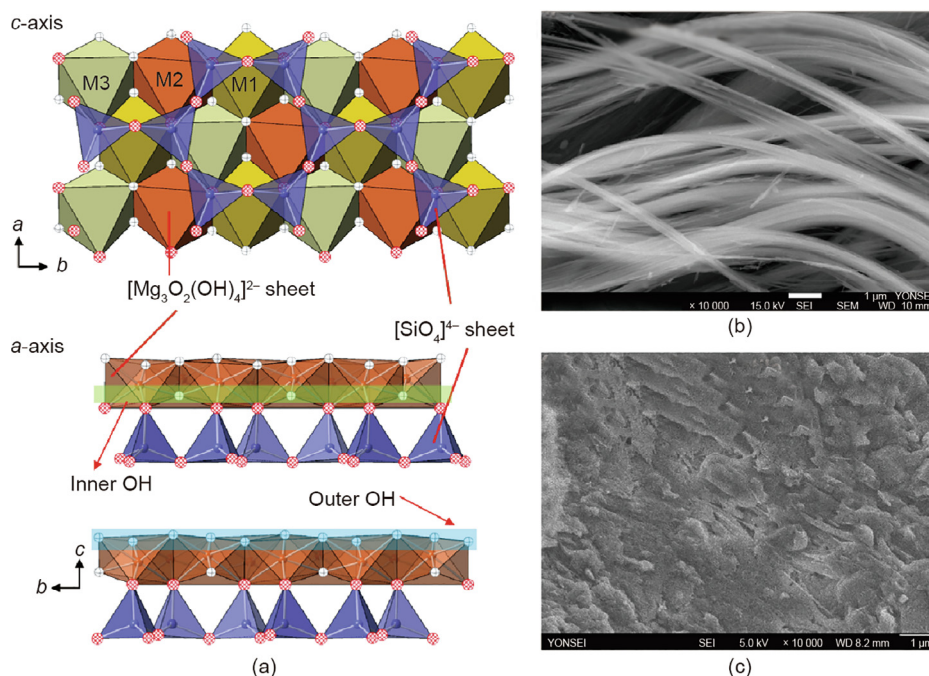
Fig. 1. (a) Crystal structural model of chrysotile ($Mg_3Si_2O_5(OH)_4$) viewed along the *c*-axis (above) and *a*-axis (below) under ambient conditions. Scanning electron microscopy (SEM) image of the chrysotile (b) under ambient conditions and (c) after reaction with carbon dioxide at high-pressure (5.32 GPa) and temperature (220 °C). M1 site refers to Mg with brucitic inheritance (HO–Mg–OH) is intercalated in between according to an azimuthal periodicity and does not chemically bond to the silica layer. M2 and M3 sites refer to octahedral Mg of the O–Si–O–Mg–OH moieties is covalently bonded to the tetrahedral of the unit cell.

the framework oxygen atoms, respectively [33]. Geometrical soft restraints on the T–O and O–O bond distances in the Si–O tetrahedron and Mg–O octahedron were applied to target values of (1.640 ± 0.001) Å and (2.692 ± 0.005) Å, and of (2.070 ± 0.001) Å and (2.001 ± 0.005) Å, respectively (Table 1). The (isothermal) bulk compressibility of the chrysotile is described by the bulk modulus K_0 ($K_0 = 1/\beta = -V \cdot \partial P / \partial V$, where β is the isothermal compressibility coefficient), obtained by a third-order Birch–Murnaghan equation of state (III-BM-EOS) fit [34], using the EOS-fit V7.0 program [35] and the data are weighted by the uncertainties in pressure (P) and volume (V).

The morphology of the sample before and after the pressure–temperature treatment was examined with a field emission scanning electron microscope (FE-SEM) using a JSM-7001F (JEOL, Japan) located at Yonsei University.

3. Results and discussion

The synchrotron XRD patterns revealed structural modifications of the chrysotile under CO_2 PTM, with drastic changes starting after heating at 170 °C for 1 h at 2.5(1) GPa (Fig. 2). These changes in the XRD patterns included the disappearance of solid CO_2 peaks and the appearance of magnesite, which indicates a pressure- and temperature-induced (partial) reaction of CO_2 PTM with the sample (Fig. 2(a)). Interestingly, after the partial carbonation reaction, the characteristic fibrous asbestos morphology of the chrysotile sample changed to an earthy form (Figs. 1(b) and (c)).

Structural models of chrysotile were derived from Rietveld refinements using synchrotron powder XRD data taken under ambient conditions and after heating at 170 °C for 1 h at 2.5 GPa. The structure of chrysotile has been reported as space group Cc and $C2/m$ for synthetic and natural samples, respectively [36,37]. Our XRD patterns are indexed in Cc, and the structural model of the chrysotile under ambient conditions shows a composition of $Mg_3Si_2O_5(OH)_4$ with unit cell constants of $a = 5.368(1)$ Å, $b = 9.201(2)$ Å, $c = 14.747(4)$ Å and $\beta = 96.25(5)°$, with the final agreement factors of $R_p = 1.64\%$, $R_{wp} = 2.66\%$, and $x^2 = 13.35$ (Tables 2 and 3). Along the a-axis, the angle between the SiT1 and SiT2 tetrahedra is refined to 65.72(1)°, and the distance between the OH2 and OH3 hydroxyl groups in the Mg octahedron at the M1 site is refined to 2.18(6) Å (Fig. 3(a)). Since OH3 is free from the silicon (Si) tetrahedron, it is prone to dehydroxylation or carbonation reactions. The angle between OH1, OH2, and OH4 is 63.91(1)°, while the occupancy of all these sites is set to 1.0 (Fig. 3(a)). When the Mg of the M1 site undergoes a carbonation

Table 1
Selected interatomic distances and angle of chrysotile under ambient and high-pressure conditions.

	Bond	Chrysotile (ambient)	Metastable chrysotile (heating at 170 °C and 2.5 GPa)
Distance (Å)	SiT1–O1	1.6522(7)	1.6390(1)
	SiT1–O2	1.6524(8)	1.6397(26)
	SiT1–O3	1.6524(8)	1.6396(30)
	SiT1–O4	1.6523(8)	1.6398(15)
	Mean	1.6523	1.6395
	SiT2–O1	1.6524(7)	1.6390(1)
	SiT2–O2	1.6524(9)	1.6397(31)
	SiT2–O3	1.6524(8)	1.6398(26)
	SiT2–O5	1.6525(8)	1.6396(13)
	Mean	1.6524	1.6395
	MgM1–O4	2.0299(8)	2.0402(28)
	MgM1–O5	2.0301(8)	2.0403(29)
	MgM1–OH1	1.9999(8)	2.0001(33)
	MgM1–OH2	2.0000(10)	2.0000(1)
	MgM1–OH3	1.9999(10)	2.0000(1)
	MgM1–OH4	2.0000(8)	2.0001(31)
	Mean	2.0100	2.0135
	MgM2–O4	2.0300(11)	2.0400(1)
	MgM2–O5	2.0301(8)	2.0403(30)
	MgM2–OH1	2.0000(11)	2.0000(1)
	MgM2–OH2	1.9999(8)	2.0000(1)
	MgM2–OH3	1.9999(8)	2.0000(1)
	MgM2–OH4	2.0000(8)	2.0001(34)
	Mean	2.0100	2.0134
	MgM3–O4	2.0306(8)	2.0401(34)
	MgM3–O5	2.0299(11)	2.0400(1)
	MgM3–OH1	2.0000(8)	2.0000(32)
	MgM3–OH2	2.0000(8)	2.0002(32)
	MgM3–OH3	2.0000(8)	2.0000(1)
	MgM3–OH4	1.9999(10)	2.0000(1)
	Mean	2.0101	2.0134
Angle (°)	O1–SiT1–O2	109.0(2)	109.2(1)
	O1–SiT1–O3	109.5(2)	109.5(1)
	O1–SiT1–O4	109.5(2)	109.5(1)
	O2–SiT1–O3	110.4(2)	110.0(1)
	O2–SiT1–O4	109.3(2)	109.3(1)
	O3–SiT1–O4	109.2(2)	109.4(2)
	O1–SiT2–O2	109.2(2)	109.2(1)
	O1–SiT2–O3	109.2(2)	109.2(1)
	O1–SiT2–O5	109.3(2)	109.6(1)
	O2–SiT2–O3	110.5(2)	110.0(1)
	O2–SiT2–O5	109.3(2)	109.4(2)
	O3–SiT2–O5	109.5(2)	109.4(1)
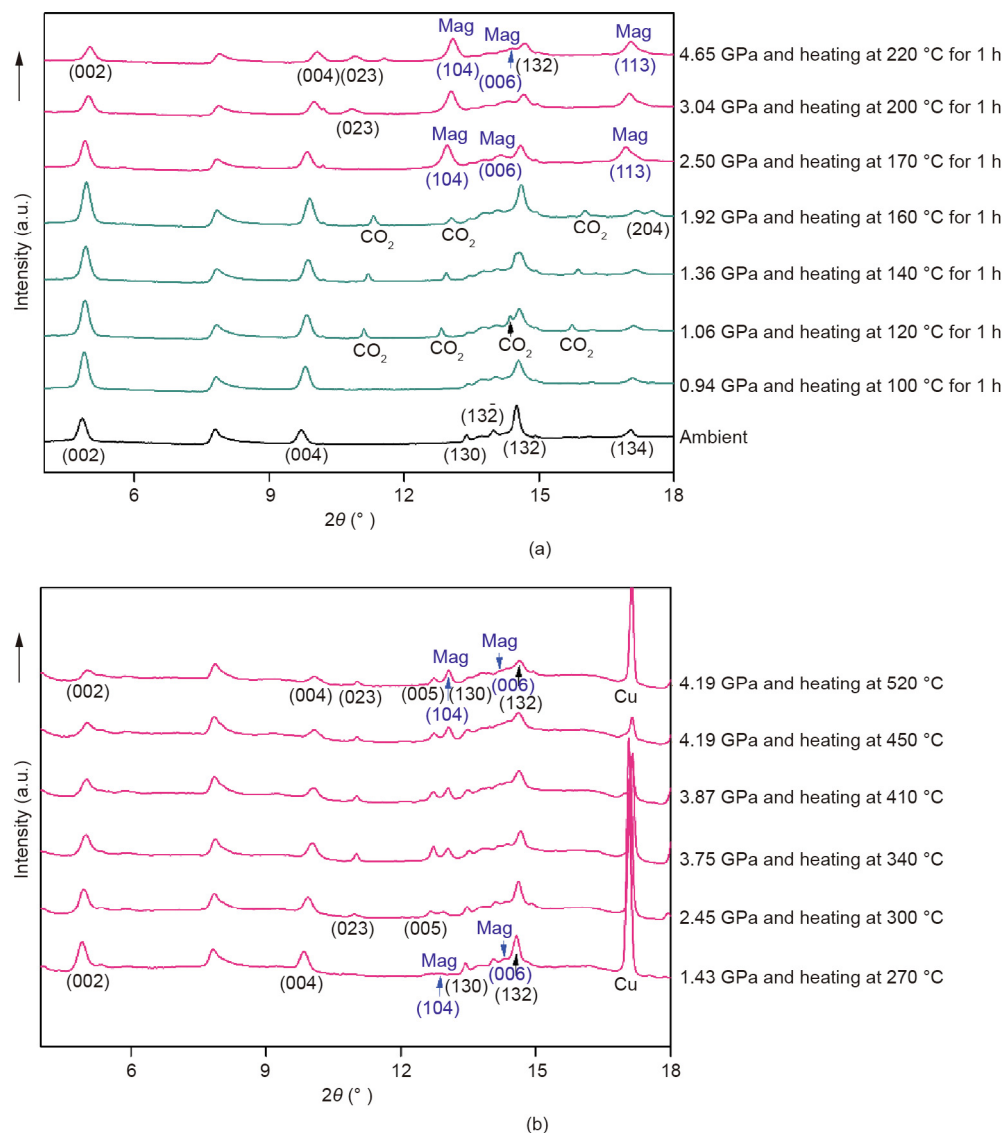
Fig. 2. Pressure-induced changes in the (a) *ex situ* and (b) *in situ* high-pressure and high-temperature synchrotron XRD patterns measured on chrysotile under carbon dioxide as a PTM at the beamline 10C at the PAL and at the beamline 16BMD of the HPCAT at the Advanced Photon Source. Mag: magnesite ($MgCO_3$).

Table 2
The structure parameters of chrysotile under ambient and high-pressure conditions.

		Chrysotile (ambient)	Metastable chrysotile (heating at 170 °C and 2.5 GPa)
Space group		Cc	Cc
R_{wp} (%)		2.66	3.09
Unit cell composition		$Mg_3Si_2O_5(OH)_4$	$Mg_{2.4(1)}Si_2O_{7.4(1)}H_{2.4(1)}$
Cell parameters	a (Å)	5.368(1)	5.355(2)
	b (Å)	9.201(2)	9.178(2)
	c (Å)	14.747(4)	14.535(2)
	β (°)	96.25(5)	96.28(5)
Cell volume V (Å^3)		724.1(3)	710.1(2)

reaction, the octahedron around the M1 site is affected. The refined composition of chrysotile after heating at 170 °C for 1 h at 2.5 GPa is then changed to $Mg_{2.4(1)}Si_2O_5(OH)_{2.4(1)}$ in the same space group Cc with lattice constants $a = 5.355(2)$ Å, $b = 9.178(2)$ Å, $c = 14.535(2)$ Å, and $\beta = 96.25(5)°$, with the final agreement factors of $R_p = 1.98\%$, $R_{wp} = 3.09\%$, and $x^2 = 15.59$ (Tables 2 and 3).

Compared with the ambient model, the occupancies of the M1 and OH3 sites have been reduced by about 50(1)%, reflecting the formation of magnesite. As a result, the distance between OH2 and OH3 in the Mg octahedron at the M1 site decreases to 1.99(1) Å, while the angle between OH1, OH2, and OH4 increases to 65.08(1)° along the *a*-axis (Fig. 3(b)). We suspect that this is

Table 3
Refined atomic positional, occupancy, and displacement parameters of chrysotile under ambient and high-pressure conditions.

Site	Parameters	Chrysotile (ambient)	Metastable chrysotile (heating at 170 ℃ and 2.5 GPa)
MgM1	x	0.926(4)	0.947(7)
	y	0.193(1)	0.189(9)
	z	0.237(2)	0.242(2)
	U_{iso}	0.013(1)	0.032(1)
	Occu.	1.000(1)	0.486(1)
MgM2	x	0.340(3)	0.373(3)
	y	0.360(2)	0.376(6)
	z	0.226(3)	0.232(1)
	U_{iso}	0.013	0.032(1)
	Occu.	1.000(1)	0.893(1)
MgM3	x	0.867(2)	0.879(9)
	y	0.503(2)	0.515(1)
	z	0.218(2)	0.212(2)
	U_{iso}	0.013(1)	0.032(1)
	Occu.	1.000(1)	1.000(1)
SiT1	x	0.003(2)	−0.004(4)
	y	0.352(2)	0.351(1)
	z	0.0412(3)	0.037(7)
	U_{iso}	0.012(1)	0.011(1)
	Occu.	1.000(1)	1.000(1)
SiT2	x	0.494(2)	0.491(1)
	y	0.521(2)	0.521(1)
	z	0.0413(3)	0.037(7)
	U_{iso}	0.012(1)	0.011(1)
	Occu.	1.000(1)	1.000(1)
O1	x	0.028(2)	0.014(4)
	y	0.216(2)	0.186(1)
	z	0.718(2)	−0.005(5)
	U_{iso}	0.034(1)	0.203(1)
	Occu.	1.000(1)	1.000(1)
O2	x	0.216(2)	0.215(5)
	y	0.457(2)	0.453(1)
	z	0.002(1)	−0.001(1)
	U_{iso}	0.034(1)	0.203(1)
	Occu.	1.000(1)	1.000(1)
O3	x	0.718(2)	0.717(7)
	y	0.415(2)	0.419(9)
	z	0.010(1)	0.005(5)
	U_{iso}	0.034(1)	0.203(1)
	Occu.	1.000(1)	1.000(1)
O4	x	0.051(5)	0.040(1)
	y	0.347(3)	0.344(1)
	z	0.154(3)	0.151(1)
	U_{iso}	0.034(1)	0.203(1)
	Occu.	1.000(1)	1.000(1)
O5	x	0.516(4)	0.517(7)
	y	0.530(3)	0.529(9)
	z	0.154(3)	0.151(1)
	U_{iso}	0.034(1)	0.203(1)
	Occu.	1.000(1)	1.000(1)
OH1	x	0.736(4)	0.735(5)
	y	0.348(2)	0.353(1)
	z	0.295(2)	0.282(1)
	U_{iso}	0.034(1)	0.203(1)
	Occu.	1.000(1)	0.174(1)
OH2	x	0.287(5)	0.311(1)
	y	0.180(2)	0.185(1)
	z	0.287(2)	0.292(1)
	U_{iso}	0.034	0.203(1)
	Occu.	1.000(1)	0.415(1)
OH3	x	0.564(5)	0.574(4)
	y	0.178(3)	0.200(3)
	z	0.189(2)	0.223(1)
	U_{iso}	0.034(1)	0.203(1)
	Occu.	1.000(1)	0.506(1)

Table 3 (*continued*)

Site	Parameters	Chrysotile (ambient)	Metastable chrysotile (heating at 170 °C and 2.5 GPa)
OH4	x	0.219(3)	0.210(1)
	y	0.528(2)	0.545(1)
	z	0.275(2)	0.289(1)
	U_{iso}	0.034(1)	0.203(1)
	Occu.	1.000(1)	0.840(1)

x, y, and z indicate relative position a specific atom in the unit cell; x is fraction of a axis, y is fraction of b axis, and z is fraction of c axis. Occu. refers to occupancy, which indicates what fraction of a site is occupied by a specific atom. U_{iso} indicates isotropic thermal parameter.
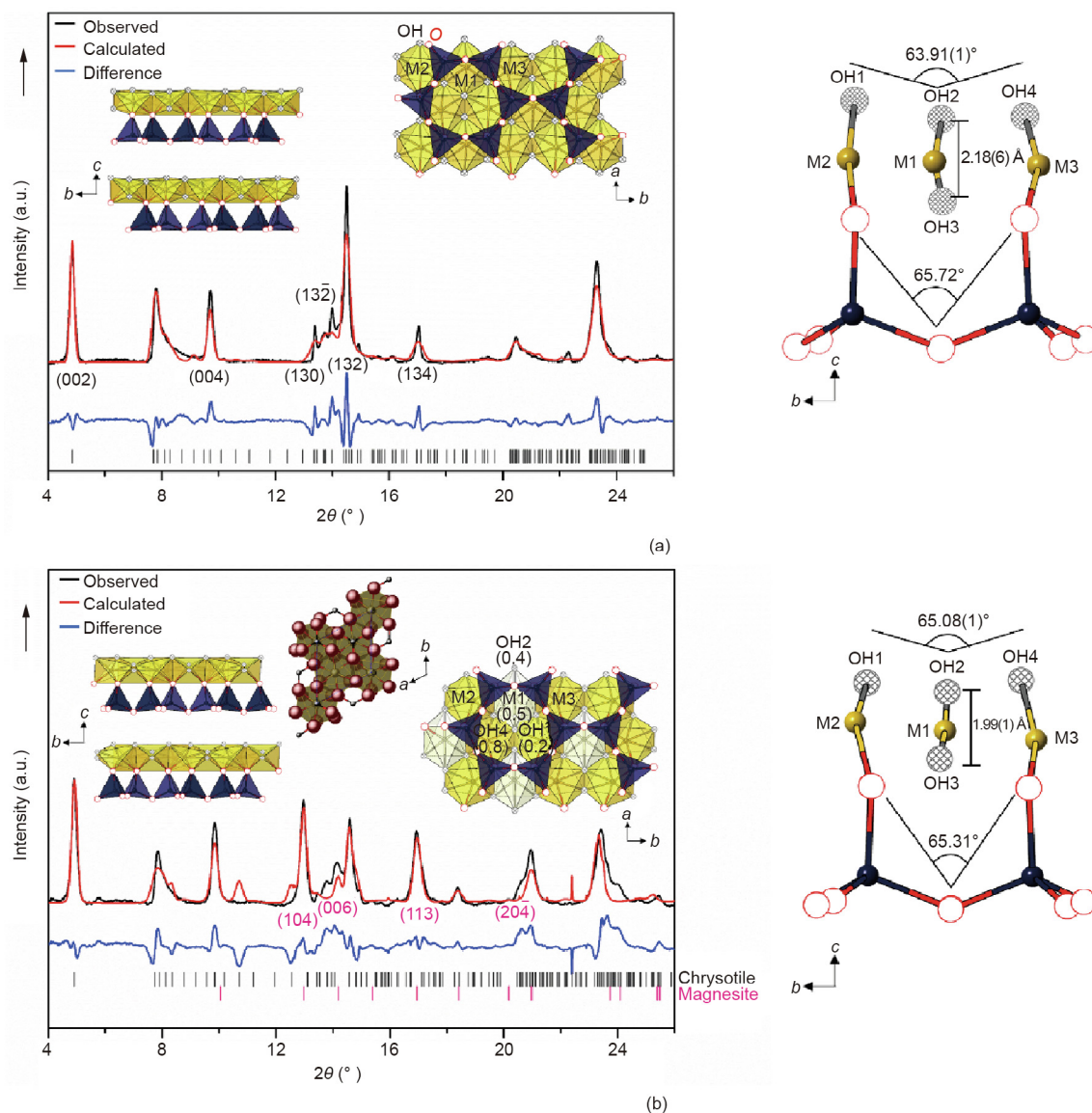

Fig. 3. Rietveld fit and derived structural details of chrysotile (a) under ambient conditions and (b) after heating at 170 °C and 2.5 GPa.

because the M1 site is bound to the OH3 site, whereas the M2 and M3 sites are connected to the Si tetrahedron (Fig. 3). Upon the formation of magnesite, the occupancies of the MgM1 octahedral site decrease to 0.49(1) and the occupancies of the hydroxyl group sites decrease to OH1 = 0.2(1), OH2 = 0.4(2), OH3 = 0.5(1), and OH4 = 0.8(4) (Fig. 3(b)).

As suggested by the mechanistic model of chrysotile dehydroxylation and carbonation [38,39], we suspect that a proton-transfer

reaction occurs upon the formation of metastable chrysotile and magnesite after heating at 170 °C for 1 h at 2.5 GPa. Incipient structural water is released from the chrysotile *T–O* unit via proton-transfer monodehydroxylation of its outermost hydroxyl groups, OH1 and OH2 [40]. This reaction would occur at the expense of the proton in the innermost hydroxyl group, OH3. The proton would then move upward continuously, and it would be much easier to fill the dehydrogenated oxygens on the left side of the vacancy. In this

intermediate state, unit cell rearrangement would presumably give rise to the metastable monodehydroxylated chrysotile intermediate, leading to the unit cell formula $Mg_{2.4(1)}Si_2O_5(OH)_{2.4(1)}$, as in Reaction (1) below.

$$Mg_3Si_2O_5(OH)_4 + CO_2 \rightarrow MgCO_3 + H_2O$$
$$+ Mg_{2.4(1)}Si_2O_5(OH)_{2.4(1)} \quad (1)$$
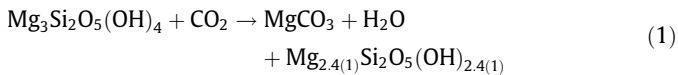
This reaction continues up to 520 °C, but thermal decomposition of chrysotile generally occurs above 660 °C. Based on previous study [41], we expect the metastable chrysotile to decompose at temperatures above 520 °C.

Our experimental conditions are comparable with the cold subduction environments of the South Sumatra and Ryukyu subduction zones [42] (Fig. 4). Chrysotile is present up to 2 GPa, while magnesite and metastable chrysotile are formed after heating at 170 °C at 2.5 GPa and maintained up to 5 GPa. It is known that chrysotile dehydrates between 5 and 8 GPa (150 and 250 km depth) above 600 °C, releasing about 13 wt% water [43]. According to recent investigation, CO_2 is lost at depths ranging from 80 to 120 km, and is then released to the atmosphere through arc-volcanism [44,45]. Our observation of serpentine carbonation closely matches this depth range.

4. Conclusion

Serpentines are a relatively stable group of minerals that exist under a wide range of temperatures and pressures from the Earth's surface down to subduction zones [46]. In this work, we reported the CO_2 interaction with chrysotile up to 5.0(1) GPa and 520 °C.
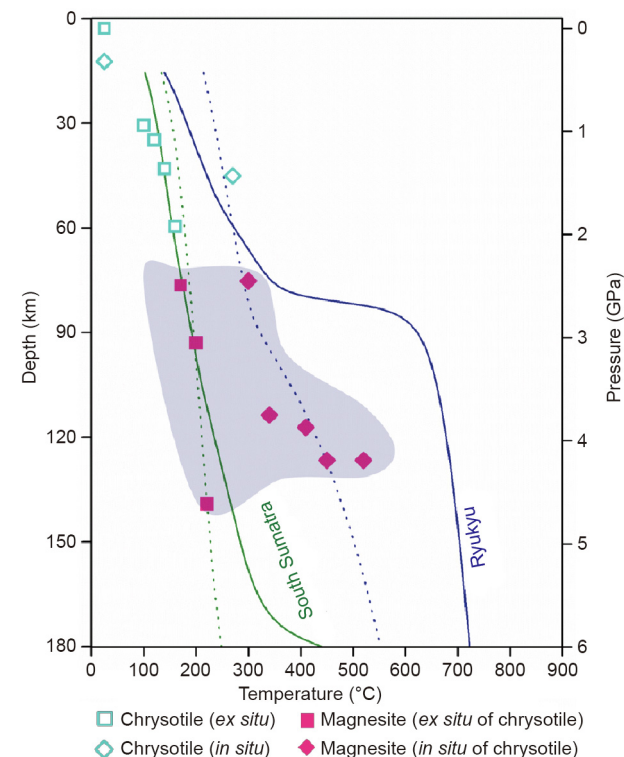
Fig. 4. Pressure–temperature paths of the slab surface (solid lines) and 7 km beneath the surface (slab Moho, dotted lines) for the South Sumatra and Ryukyu subduction zones. The square symbols show high-pressure data after heat treatment. (Diamond symbols indicate *in situ* high-pressure and high-temperature experiments, and filled symbols represent a mixture of metastable chrysotile and magnesite.)

Under ambient conditions, chrysotile changes to metastable chrysotile upon partial carbonation to magnesite at a depth of about 80 km under cold subduction conditions; this is in line with the proposed carbon cycle, leading to arc-volcanism. Interestingly, the characteristic fibrous morphology of chrysotile changes into an earthy form upon the carbonation reaction. This finding carries potential for use as a possible detoxification method for asbestos using moderate pressure and temperature. Further studies are under way to understand the stability of metastable chrysotile under higher pressure and temperature conditions.

Compliance with ethics guidelines

Mihye Kong and Yongjae Lee declare that they have no conflict of interest or financial conflicts to disclose.

References

[1] Keil K. Mineralogical and chemical relationships among enstatie chondrites. J Geophys Res 1968;73(22):6945–76.
[2] Takahashi T, Sutherland SC, Kozyr A. Global ocean surface water partial pressure of CO_2 database: measurements performed during 1957–2012. Report. Tennessee: Carbon Dioxide Information Analysis Center, Oak Ridge National Laboratory, US Department of Energy; 2012.
[3] Alt JC, Teagle DAH. The uptake of carbon during alteration of ocean crust. Geochim Cosmochim Acta 1999;63(10):1527–35.
[4] Charvrit D, Humler E, Grasset O. Mapping modern CO_2 fluxes and mantle carbon content all along the mid-ocean ridge system. Earth Planet Sci Lett 2014;387:229–39.
[5] Sleep NH, Zhanle K. Carbon dioxide cycling and implications for climate on ancient Earth. J Geophys Res 2001;106(E1):1373–99.
[6] Dasgupta R, Hirschmann MM. The deep carbon cycle and melting in Earth's interior. Earth Planet Sci Lett 2010;298(1–2):1–13.
[7] Plank P, Langmuir CH. The chemical composition of subducting sediment and its consequences for the crust and mantle. Chem Geol 1998;145(3–4): 325–94.
[8] Staudigel H. Hydrothermal alteration processes in the oceanic crust. In: Holland HD, Turekian KK, editors. Treatise on geochemistry. Oxford: Elsevier-Pergamon; 2003. p. 511–35.
[9] Shilobreeva S, Martinez I, Busigny V, Agrinier P, Laverne C. Insights into C and H storage in the altered oceanic crust: results from ODP/IODP Hole 1256D. Geochim Cosmochim Acta 2011;75(9):2237–55.
[10] Debret B, Koga KT, Cattani F, Nicollet C, den Bleeken GV, Tchwartz S. Volatile (Li, B, F and Cl) mobility during amphibole breakdown in subduction zones. Lithos 2016;244:165–81.
[11] Power IM, Wilson SA, Dipple GM. Serpentinite carbonation for CO_2 sequestration. Elements 2013;9(2):115–21.
[12] Poli S, Schmidt MW. Water transport and release in subduction zones: experimental constraints on basaltic and andesitic systems. J Geophys Res 1995;100(B11):22299–314.
[13] Wunder B, Schreyer W. Antigorite: high pressure stability in the system MgO–SiO_2–H_2O (MSH). Lithos 1997;41(1–3):213–27.
[14] Grove TL, Till CB, Lev E, Chatterjee N, Médard E. Kinematic variables and water transport control the formation and location of arc volcanoes. Nature 2009;459(7247):694–7.
[15] Magni V, Bouilhol P, van Hunen J. Deep water recycling through time. Geochem Geophys Geosyst 2014;15(11):4203–16.
[16] Molina JF, Poli S. Carbonate stability and fluid composition in subducted oceanic crust: an experimental study on H_2O-CO_2-bearing basalts. Earth Planet Sci Lett 2000;176(3–4):295–310.
[17] Kerrick DM, Connolly JAD. Metamorphic devolatilization fo subducted mid-ocean ridge matabasalts: implications for seismicity, arc magmatism and volatile recycling. Earth Planet Sci Lett 2001;189(1–2):19–29.
[18] Kiseeva ES, Yaxley GM, Hermann J, Litasov KD, Rosenthal A, Kamenetsky VS. An experimental study of carbonated eclogite at 3.5–5.5 GPa-implications for silicate and carbonate metasomatism in the cratonic mantle. J Petrol 2012;53:727–59.

[19] Dorogokupers PI. Equation of state of magnesite for the conditions of the Earth's lower mantle. Geochem Int 2007;45(6):561–8.
[20] Ulmer P, Trommsdorff V. Phase relations of hydrous mantle subducting to 300 km. In: Fei Y, Bertka CM, Mysen BO, editors. Mantle petrology: field observations and high pressure experimentation. Houston: Geochemical Society Special Publication; 1999. p. 259–81.
[21] Bostock MG, Hyndman RD, Rondenay S, Peacock SM. An inverted continental Moho and serpentinization of the forearc mantle. Nature 2002;417 (6888):536–8.
[22] Rupke LH, Morgan JP, Hort M, Connolly JAD. Serpentine and the subduction zone water cycle. Earth Planet Sci Lett 2004;223(1–2):17–34.
[23] Fryer P, Ambos EL, Hussong DM. Origin and emplacement of Mariana forearc seamounts. Geology 1985;13(11):774–7.
[24] Guillot S, Hattori K, de Sigoyer J, Nagler T, Auzende AL. Evidence of hydration of the mantle wedge and its role in the exhumation of eclogites. Earth Planet Sci Lett 2001;193(1–2):115–27.
[25] Dobson DP, Meredith PG, Boon SA. Simulation of subduction zone seismicity by dehydration of serpentine. Science 2002;298(5597):1407–10.
[26] Jung H, Green II HW, Dobrzhinetskaya LF. Intermediate-depth earthquake faulting by dehydration embrittlement with negative volume change. Nature 2004;428(6982):545–9.
[27] Evans BW. The serpentinite multisystem revisited: chrysotile is metastable. Int Geol Rev 2004;46(6):479–506.
[28] Reynard B, Hilairet N, Balan E, Lazzeri M. Elasticity of serpentines and extensive serpentinization in subduction zones. Geophys Res Lett 2007;34 (13):L13307.
[29] Mao HK, Xu J, Bell PM. Calibration of the ruby pressure gauge to 800 kbar under quasi-hydrostatic conditions. J Geophys Res 1986;91(B5):4673–6.
[30] Larson AC, Von Dreele RB. General structure analysis system (GSAS). Report. Los Alamos: Los Alamos National Laboratory; 2004.
[31] Toby BH. EXPGUI, a graphical user interface for GSAS. J Appl Cryst 2001;34 (2):210–3.
[32] Thompson P, Cox DE, Hastings JB. Rietveld refinement of Debye–Scherrer synchrotron X-ray data from Al$_2$O$_3$. J Appl Cryst 1987;20(2):79–83.
[33] Rietveld HM. A profile refinement method for nuclear and magnetic structures. J Appl Cryst 1969;2(2):65–71.
[34] Birch F. Finite elastic strain of cubic crystals. Phys Rev 1947;71(11): 809–24.
[35] Angel RJ, Gonzalez-Platas J, Alvaro M. EosFit-7c and a fortran module (library) for equation of state calculations. Z Kristallogr 2014;229:405–19.
[36] Gualtieri AF, Artioli G. Quantitative determination of chrysotile asbestos in bulk materials by combined Rietveld and RIR methods. Powder Diffr 1995;10 (4):269–77.
[37] Falini G, Foresti E, Gazzano M, Gualtieri AF, Leoni M, Lesci IG, et al. Tubular-shaped stoichiometric chrysotile nanocrystals. Chemistry 2004;10 (12):3043–9.
[38] Kalinichenko EA, Litovchenko AS. Effect of an electric field on brucite dehydroxylation. Phys Solid State 2000;42(11):2070–5.
[39] Mckelvy MJ, Sharma R, Chizmeshya AVG, Carpenter RW, Streib K. Magnesium hydroxide dehydroxylation: in situ nanoscale observation of lamellar nucleation and growth. Chem Mater 2001;13(3):921–6.
[40] Larachi F, Daldoul I, Beaudoin G. Fixation of CO$_2$ by chrysotile in low-pressure dry and moist carbonation: ex-situ and in-situ characterizations. Geochim Cosmochim Acta 2010;74(11):3051–75.
[41] Dlugogorski BZ, Balucan RD. Dehydroxylation of serpentine minerals: implications for mineral carbonation. Renew Sustain Energy Rev 2014;34:353–67.
[42] Clift P, Vannucchi P. Controls on tectonic accretion versus erosion in subduction zones: implications for the origin and recycling of the continental crust. Rev Geophys 2004;42(2):RG2001.
[43] Obara K. Nonvolcanic deep tremor associated with subduction in southwest Japan. Science 2002;296(5573):1679–81.
[44] Syracuse EM, van Keken PE, Abers GA. The global range of subduction zone thermal models. Phys Earth Planet Inter 2010;183(1–2):73–90.
[45] Van Keken PE, Hacker BR, Syracuse EM, Abers GA. Subduction factory: 4. depth-dependent flux of H$_2$O from subducting slabs worldwide. J Geophys Res 2011;116(B1):B01401.
[46] Guillot S, Schwartz S, Reynard B, Agard P, Prigent C. Tectonic significance of serpentinites. Tectonophysics 2015;646:1–19.